Effect of Cooling Rate on Nucleation Behavior of Milk Fat−Sunflower Oil Blends

S. Martini,[†] M. L. Herrera,[†,§] and R. W. Hartel*[,‡]

Centro de Investigación y Desarrollo en Criotecnología de Alimentos, Calle 47 y 116, 1900 La Plata, Buenos Aires, Argentina, and Food Science Department, University of Wisconsin−Madison, 1605 Linden Drive, Madison, Wisconsin 53706

The effect of cooling rate on the crystallization behavior of mixes of high-melting milk fat fraction (HMF) and sunflower oil (SFO) was studied by following nucleation with laser-polarized turbidimetry. The initial crystals were photographed, and their thermal and polymorphic behaviors, as well as chemical composition, were investigated by calorimetry, X-ray diffraction, and capillary gas chromatography. Activation energies of nucleation were calculated using the Fisher−Turnbull equation. Despite small differences in Mettler dropping points for different ratios of SFO to HMF, induction times were significantly different between samples and were shorter at a slow cooling rate for the same supercooling. Rapidly cooled samples required more time at crystallization temperature to crystallize than slowly cooled samples because molecular organization prior to nuclei formation took place under different conditions. Regardless of cooling rate or composition, all crystals were in the β' polymorph. However, morphology, thermal behavior, and chemical composition showed differences with cooling rate. Activation free energies of nucleation were of the same order of magnitude as those published for hydrogenated SFO.

Keywords: *High-melting milk fat fraction; sunflower oil; cooling rate; nucleation; induction time; activation free energy; polymorphism; morphology; thermal behavior*

INTRODUCTION

Crystallization studies are important from both technological and academic points of view. Understanding the effects of formulation and process factors on the kinetics of crystallization is important to control of product quality.

Milk fat contains the most complex lipid composition of the natural fats. Triacylglycerols (TAG) comprise by far the greatest proportion of lipids in milk fat, making up 97−98% of the total lipid. The other components included are diacylglycerols (DAG), monoacylglycerols (MAG), free fatty acids, free sterols, and phospholipids (*1*). Due to its complex composition, the melting range of milk fat is broad, spanning from about −40 to 40 °C. Furthermore, the composition changes with season, region, and diet.

To extend the use of milk fat in food, pharmaceutical, and cosmetic applications, fractionation may be performed to produce components with specific properties (e.g., melting point). Milk fat fractions are also blended to give a manufacturer greater flexibility to tailor milk fat as an ingredient to specific functional requirements than could be accomplished with fractionation alone (*2*).

Crystallization in general can be divided into two steps: nucleation and growth. Before nuclei formation, the mother phase must be supercooled to provide a thermodynamic driving force for crystallization (*3*). Once the nuclei have formed, they grow and develop into crystals. In fact, both events usually happen simultaneously and the system is in continuous evolution. Additional changes in crystals can occur as stable crystals modify their habit and metastable crystals undergo polymorphic transitions (*4*).

Nucleation studies have been performed previously on different fat systems. Induction times of crystallization were measured by light-polarized microscopy and by laser light-polarized turbidimetry. Activation free energies of nucleation were calculated from the Fisher−Turnbull equation for different supercoolings in vegetable oils (palm and hydrogenated sunflower oils) and in milk fat model systems [blends of different proportions of high-melting (HMF) and low-melting (LMF) fractions of milk fat] (*5*−*8*). Thus, to increase understanding of the variable kinetics of crystallization in HMF and vegetable oil blends, the present study analyzes the effect of cooling rate on the kinetics of nucleation in these systems. Polymorphism, morphology, and thermal behavior of the crystals were also studied.

MATERIALS AND METHODS

Starting Systems. HMF was obtained from La Serenisima S.A. (Gral. Rodríguez, Buenos Aires, Argentina) and sunflower oil (SFO) from Molinos Rio de La Plata S.A. (Avellaneda, Buenos Aires, Argentina). Three systems were prepared by mixing 10, 20, and 40% (w/w) SFO with HMF. The melting points (T_m), measured as Mettler dropping points (MDP), and TAG compositions of the HMF, SFO, and three blends are reported in Table 1.

Laser-Polarized Light Turbidimetry. The crystallization process was monitored by using an optical setup described elsewhere (*9*). A laser-polarized turbidimeter with a helium−

* Author to whom correspondence should be addressed [telephone +1 (608) 263 1965; fax +1 (608) 262 6872; e-mail hartel@calshp.cals.wisc.edu].

[†] Centro de Investigación y Desarrollo en Criotecnología de Alimentos (UNLP-CONICET).

[§] Researcher of the National Research Council.

[‡] University of Wisconsin−Madison.

10.1021/jf001101j CCC: $20.00
Published on Web 06/12/2001

Table 1. Chemical Composition and Mettler Dropping Points (MDP) of the Fats

	chemical composition of starting materials (wt %)				
acyl C no.	SFO	HMF	10% SFO	20% SFO	40% SFO
C26	0.3 ± 0.2	0.5 ± 0.4	0.5 ± 0.3	0.4 ± 0.3	0.4 ± 0.2
C28	0.0 ± 0.0	0.5 ± 0.3	0.5 ± 0.4	0.4 ± 0.2	0.4 ± 0.3
C30	0.0 ± 0.0	1.0 ± 0.7	0.9 ± 0.7	0.8 ± 0.4	0.7 ± 0.5
C32	0.0 ± 0.0	2.1 ± 0.5	2.0 ± 0.5	1.8 ± 0.7	1.4 ± 0.5
C34	0.0 ± 0.0	4.8 ± 0.7	4.4 ± 0.7	3.9 ± 0.7	3.2 ± 0.7
C36	0.3 ± 0.2	8.6 ± 0.6	7.9 ± 0.5	7.2 ± 0.6	6.3 ± 0.7
C38	3.9 ± 0.4	13.2 ± 0.7	12.4 ± 0.7	11.4 ± 0.5	7.8 ± 0.5
C40	0.0 ± 0.0	8.0 ± 0.7	7.3 ± 0.4	6.6 ± 0.6	7.2 ± 0.6
C42	0.0 ± 0.0	7.0 ± 0.5	6.1 ± 0.5	5.5 ± 0.7	4.2 ± 0.4
C44	0.0 ± 0.0	7.5 ± 0.6	6.5 ± 0.7	5.8 ± 0.6	4.8 ± 0.3
C46	0.0 ± 0.0	9.0 ± 0.5	6.6 ± 0.6	6.9 ± 0.7	5.8 ± 0.3
C48	0.1 ± 0.2	11.0 ± 0.7	10.0 ± 0.7	8.3 ± 0.5	6.8 ± 0.3
C50	2.2 ± 0.4	13.2 ± 0.5	12.5 ± 0.7	10.3 ± 0.4	8.8 ± 0.5
C52	20.1 ± 0.8	9.2 ± 0.7	10.0 ± 0.5	9.9 ± 0.5	13.1 ± 0.7
C54	73.1 ± 0.7	4.3 ± 0.5	12.5 ± 0.7	20.6 ± 0.7	29.3 ± 0.6
C54 (18:0)-d	0.8 ± 0.5	0.3 ± 0.2	1.4 ± 0.3	0.3 ± 0.2	0.5 ± 0.4
C54 (18:1)-a,b,c	72.3 ± 0.7	3.9 ± 0.5	11.1 ± 0.6	20.3 ± 0.8	28.8 ± 0.7
C54-b (unknown)	4.5 ± 0.8	1.5 ± 0.5	1.0 ± 0.7	2.6 ± 0.5	4.3 ± 0.2
C54-c (unknown)	0.0 ± 0.0	1.0 ± 0.7	1.9 ± 0.4	0.9 ± 0.3	0.2 ± 0.3
C54 (18:1cis)-a	67.8 ± 0.5	1.5 ± 0.4	8.1 ± 0.5	16.9 ± 0.5	24.3 ± 0.5
MDP (°C)		40.2 ± 0.7	40.4 ± 0.7	38.8 ± 0.6	37.4 ± 0.6

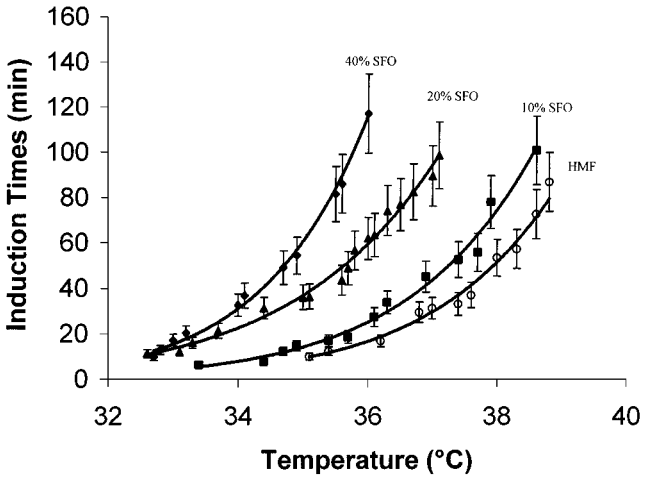

Figure 1. Induction times of crystallization vs temperature for rapidly crystallized samples (5.5 °C/min): (◆) 40%, (▲) 20%, and (■) 10% SFO blends; (○) HMF sample. Data points are the average of three runs. Error bars are standard deviations. Significant differences were found between HMF and 10% SFO and between 10 and 20% SFO ($p < 0.05$), and between 20 and 40% SFO ($p < 0.01$).

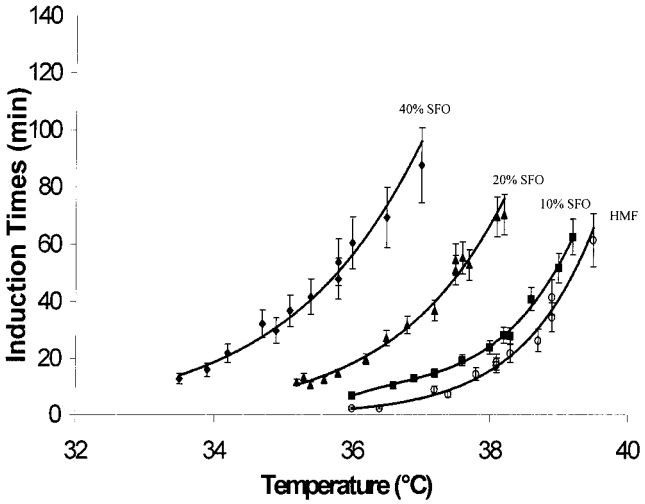

Figure 2. Induction times of crystallization vs temperature for slowly crystallized samples (0.1 °C/min): (◆) 40%, (▲) 20%, and (■) 10% SFO blends; (○) HMF sample. Data points are the average of three runs. Error bars are standard deviations. Statistical analysis as Figure 1.

neon laser as light source was used to follow the occurrence of optically anisotropic fat crystals. The sample, ~80 g, was contained in a water-jacketed glass cell. A polarizer lens was placed between the laser and the cell. The temperature of the glass cell was controlled by means of water that was circulated from a water bath. The light transmitted by the crystals was then passed through the second analyzer placed at the Cross−Nicolls position with the first analyzer; this enables the photodiode to detect crystals. A typical photosensor output and the cell temperature record were reported previously (*9*). Induction time of crystallization (τ) is defined as the interval between the moment crystallization temperature (T_c) is reached and the start of crystallization (first deviation from the laser baseline signal).

Thermal Treatments. Samples in the glass cell, mechanically stirred by a magnetic stirrer at a fixed speed (150 rpm), were crystallized at two cooling rates: 5.5 °C (fast rate) and 0.1 °C/min (slow rate). Samples were melted and held at 80 °C for 30 min and then immediately placed at the T_c reported in Figure 1 (fast rate) or cooled from 60 °C to the T_c reported in Figure 2 at 0.1 °C/min using a programmable LAUDA ethyleneglycol/water (3:1) bath model RK 8 KP (Werklauda, Königshofen, Germany). The fast cooling rate was calculated from the slope of the cell temperature record, and the results of several runs were averaged. Each of the two thermal treatments was carried out in triplicate, and induction times were reported as the average.

Isothermal Crystallization. The initial crystals, which are defined as the crystals present in the cell when the laser signal reaches the maximum (*9*), were observed under a polarized light optical microscope. At the completion of a run, the sample was filtered under vacuum with a Büchner filter using Whatman no. 4 filter paper. The solids were then analyzed for their polymorphic form by X-ray diffractometry (XRD), for their thermal behavior by differential scanning calorimetry (DSC), and for their chemical composition by capillary gas chromatography (CGC).

Optical Microscopy. A Leitz microscope model Ortholux II (Ernest Leitz Co., Wetzlas, Germany) with a controlled-temperature platform was used to photograph the initial crystals. The platform temperature was controlled by a Lauda TUK cryostat (Werklauda). Crystals were collected with a pipet from the cell and were placed on the slide at crystallization temperature. Photographs of the crystals were taken with a Leitz-Vario-Othomat camera under polarized light. Magnification of 250× was used for all photographs.

XRD. Samples were analyzed for their polymorphic form by using a Philips 1730 X-ray spectrometer fitted with a system for temperature control (Philips Argentina S.A., Capital Federal, Argentina). The temperature of the sample holder placed within the refraction chamber was controlled through a programmable Lauda UK 30 cryostat (Werklauda). Ethylene glycol in water (3:1, v/v) was used as coolant. $K_{\alpha 1 \alpha 2}$ radiation from copper was used at 40 kV, 20 mA, and scanning velocity of 1°/min from 5 to 30°.

DSC. Measurements were carried out in a Polymer Laboratories calorimeter (Rheometric Scientific Ltd.) driven with Plus V 5.41 software. Calibration was carried out at a heating rate of 5 °C/min by using indium proanalysis (p.a.), lauric acid p.a., and stearic acid p.a. as standards. Samples ranging from 8 to 12 mg were placed in hermetically sealed aluminum pans and subjected to a heating rate of 5 °C/min from 0 to 80 °C. A single empty pan was employed as a reference. Three replicates were performed for each sample to obtain the mean value and a measure of the statistical dispersion of each parameter.

CGC. Acyl carbon profile was determined using a Hewlett-Packard 5890 series II (Hewlett-Packard, San Fernando, CA) gas chromatography unit equipped with a flame ionization detector (FID) and an on-column injector. The column used was a Heliflex Phase AT-1 with a length of 30 m and an internal diameter of 0.25 mm (Alltech Associates, Deerfield, IL). Helium was the carrier gas at a flow rate of 2 mL/min with hydrogen gas and air also being supplied to the FID. Samples were prepared by using a modified method of Lund (*10*). Ten milligrams of sample was weighed in GC vials and dissolved in 1.8 mL of iso-octane. One hundred microliters of internal standard [TAG with 27 carbons (C_{27} trioctanoin) in iso-octane: 2.02 mg/mL] was added to the vial. Samples were stored in a refrigerator prior to analysis. To separate the different TAG according to acyl carbon number, the following temperature profile was used: initial hold at 280 °C for 1 min, increased at a rate of 3.0 °C/min until a temperature of 355 °C was reached. The detector was held constant at 370 °C. Composition was based on the area integrated by using ChemStation Chromatography software by Hewlett-Packard. Samples were run in duplicate.

Calculation of Activation Free Energy of Nucleation. The activation free energy of nucleation, ΔG_c, was evaluated using the Fisher−Turnbull equation (*11*)

$$J = (NkT/h) \exp(-\Delta G_d/kT) \exp(-\Delta G_c/kT) \quad (1)$$

where J is the rate of nucleation, ΔG_d the activation free energy of diffusion, k the gas constant per molecule, T the temperature, N the number of molecules per cubic centimeter in the liquid phase, and h Planck's constant. J can be taken as being proportional to the inverse of the induction time (τ) of nucleation. For a spherical nucleus, the activation free energy of nucleation is related to the surface free energy of the crystal/melt interface, σ, and the supercooling (melting point − crystallization temperature) $\Delta T = (T_m - T_c)$ by

$$\Delta G_c = (16/3)\pi\sigma^3 T_m^2/(\Delta H)^2(\Delta T)^2 \quad (2)$$

with ΔH the enthalpy of nucleation.

For a triacylglycerol system, the main barrier to diffusion is the molecular conformation, and, therefore, the first exponential in eq 1 is equal to

$$-\alpha\Delta S/R \quad (3)$$

where α is the fraction of molecules that should be in the right conformation for incorporation in a nucleus, ΔS the decrease of entropy on crystallization of 1 mol of TAG, and R the gas constant. Combining eqs 1−3 and rearranging, the following equation is obtained:

$$\tau T = h/Nk \exp(\alpha\Delta S/k) \exp[(16/3)\pi\sigma^3 T_m^2/kT(\Delta H)^2(\Delta T)^2] \quad (4)$$

From a plot of ln τT versus $1/T(\Delta T)^2$ a slope (s) can be evaluated, which allows calculation of the activation free energy of nucleation from

$$\Delta G_c = sk/(T_m - T_c)^2 \quad (5)$$

Although the slope obtained from this analysis is a constant, the activation free energy is a function of supercooling. The Fisher−Turnbull equation was originally derived for a single-component system; however, it was proved to be applicable to palm and sunflower oils, which are multicomponent systems (*5*, *6*). Differences in induction times between two samples were compared using the paired Student's t test at $p < 0.01$ and $p < 0.05$.

RESULTS AND DISCUSSION

Induction Times of Crystallization. Figure 1 shows the induction times obtained when samples were crystallized at the fast cooling rate (5.5 °C/min), and Figure 2 shows the results obtained at the slow cooling rate (0.1 °C/min). Despite the small differences in melting points (measured as MDP) for different ratios of SFO to HMF (Table 1), induction times were significantly different at $p < 0.05$ between samples. At slow cooling rates, there was a significant difference ($p < 0.05$) in induction times for HMF and 10% SFO blends and for 10 and 20% SFO blends at all T_c; there was a significant difference ($p < 0.01$) for 20 and 40% SFO samples. Induction times were shorter at the slow cooling rate for the same supercooling, which is somewhat surprising. In general, when a fat is crystallized at a fast cooling rate (80 °C/min to a temperature below T_m of the α-polymorph), the α-polymorph can be expected, whereas at the rates used in this study (i.e., 0.1 °C/min), the β' or β polymorph is expected (*12*). When palm oil was cooled at 0.1 °C/min to crystallization temperatures close to the melting point, the β'-form had a shorter induction time than the β-form. For the three main polymorphic forms of fats, induction times increase in the order α, β', and β (*13*). A slower cooling rate might be expected to promote the formation of more stable forms (β polymorph), which have longer induction times. However, the results obtained in this study were reversed, with the faster cooling rate giving longer induction times. The thermodynamic driving force was the same in both cases, but rapidly cooled samples (5.5 °C/min) took longer at each temperature to crystallize. Similar results were also found for hydrogenated sunflower seed oil, which has very different chemical characteristics (rich in elaidic acid TAG; *9*).In nucleation, molecules need sufficient time to organize and align with their neighbors to form stable nuclei. In the rapidly cooled sample, that organization took place primarily at crystallization temperature, whereas the slower cooling process allowed reorganization to occur at warmer temperatures as the sample was cooling to crystallization temperature. The end result was that the sample that was cooled slowly needed less time at crystallization temperature to nucleate because much of the molecular organization had already taken place by the time it reached crystallization temperature.

For all samples and for both cooling rates, a continuous curve can be drawn for induction time versus temperature. This means that when samples were crystallized at these temperatures, only one polymorphic form was obtained. These results were confirmed by analyzing the initial crystals by XRD. For all samples at all T_c and for both cooling rates, only the β'-form was

Table 2. Activation Free Energies of Nucleation (ΔG_c) of All Samples

HMF			10% SFO			20% SFO			40% SFO		
T_c (°C)	ΔT (°C)	ΔG_c (kJ/mol)	T_c (°C)	ΔT (°C)	ΔG_c (kJ/mol)	T_c (°C)	ΔT (°C)	ΔG_c (kJ/mol)	T_c (°C)	ΔT (°C)	ΔG_c (kJ/mol)
37.2	3	1.2	36.9	3.5	1.1	35.6	3.2	1.6	33.5	3.9	1.3
37.8	2.4	1.9	37.2	3.2	1.3	35.8	3	1.8	33.9	3.5	1.6
38.1	2.1	2.4	37.6	2.8	1.8	36.2	2.6	2.4	34.2	3.2	2.0
38.3	1.9	3.0	38.0	2.4	2.4	36.5	2.3	3.1	34.7	2.7	2.8
38.7	1.5	4.8	38.2	2.2	2.8	36.8	2.0	4.0	34.9	2.5	3.2
			38.3	2.1	3.1				35.1	2.3	3.8
			38.6	1.8	4.2						

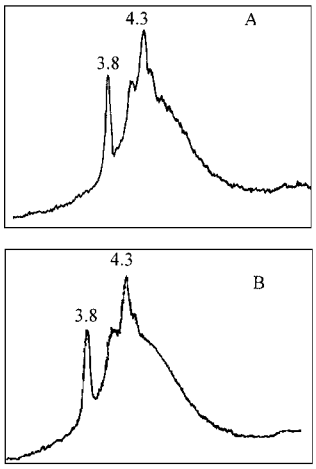

Figure 3. X-ray patterns of slowly (A) and rapidly (B) crystallized samples (10% SFO) at 36.0 °C.

found. As shown in Figure 3, the patterns were characteristic of the β'-form with two strong signals at 3.9 and 4.3 Å. No signal at 4.6 Å, characteristic of the β-form, was found. X-ray spectra for all samples were very similar and, therefore, polymorphism was not responsible for differences in induction times.

Activation Energies of Nucleation. The activation free energies (ΔG_c) of these samples, calculated from the Fisher−Turnbull equation and with the induction times measured at slow rate, are reported in Table 2 along with the crystallization temperatures and supercoolings, $\Delta T = (T_m - T_c)$, based on MDP for the samples reported in Table 1. The slopes obtained from plots of $\ln(\tau T)$ versus $1/T(\Delta T)^2$ for the HMF and 10%, 20, and 40% SFO samples were 1.302×10^3, 1.667×10^3, 1.956×10^3, and 2.439×10^3, respectively. The regression coefficients obtained from the plots are shown in Figure 4. The ΔG_c of the blends increased as the amount of HMF in the blend decreased for the same supercooling (i.e., for a ΔT of 2.4 ΔG_c values were 1.9, 2.4, 2.9, and 3.5 for HMF and 10, 20, and 40% SFO, respectively), although the values were closer than perhaps might be expected on the basis of chemical composition. The addition of sunflower oil did not have much effect on the energy barrier. For TAG, the main diffusional barrier for nucleation is the molecular structure. The TAG has to be in the right conformation before it can be incorporated in a nucleus (*12*). On the basis of the composition of the blends (Table 1), addition of SFO substantially increased the content of C18:1 in the blends. However, activation free energies were closer than expected according to the differences in C18:1 for the different blends at the same supercooling. These values were also of the same order of magnitude as those published for hydrogenated SFO, which has a high proportion of TAG with elaidic acid (*6*), and 10 times lower than values calculated for palm oil (*5*), which is a natural semisolid fat. In the HMF−SFO system, nucleation was very fast

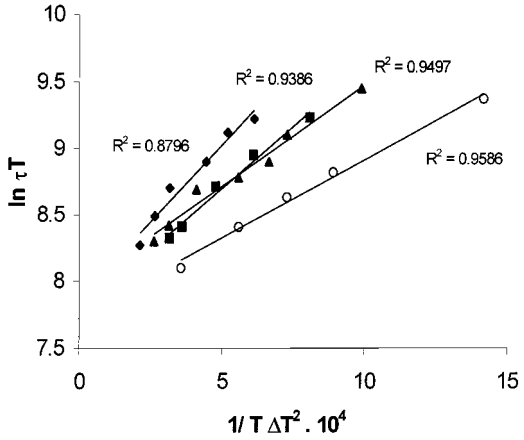

Figure 4. Plots of $\ln \tau T$ vs $1/T(\Delta T^2)$: (◆) 40%, (▲) 20%, and (■) 10% SFO blends; (○) HMF sample. τ is induction time, and T is temperature.

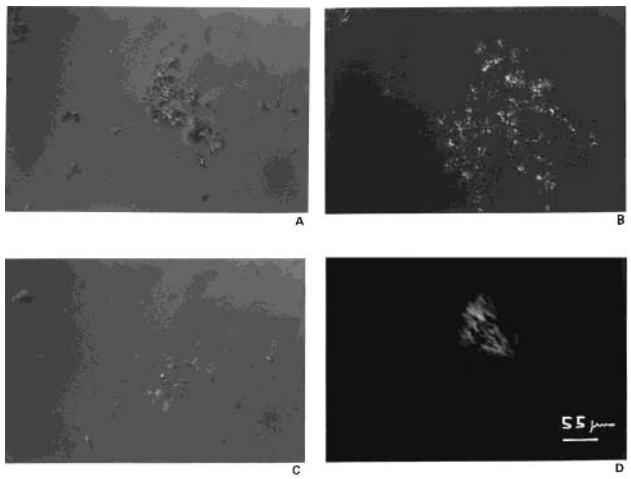

Figure 5. Morphology of initial crystals of samples crystallized to 36.0 °C: (A) HMF; (B) 10%, (C) 20%, and (D) 40% SFO at fast rates (5.5 °C/min).

and only a small supercooling was needed. Even at crystallization temperatures close to the MDP, crystallization occurred.

Morphology of Initial Crystals. Figure 5 shows the typical morphology of initial crystals, obtained when samples were crystallized at 36.0 °C with a cooling rate of 5.5 °C/min. The crystals for samples of 0, 10, and 20% SFO all had similar morphologies. Well-organized spherulitic patterns showing a needle structure were observed, with the needles organized radially outward from the center. However, the spherulites were less densely packed (lighter in color) with increased addition of SFO. The sample with 40% SFO showed a different morphology. Incomplete spherulites with larger needles were found. Crystallization at this temperature occurred at the lowest supercooling of the four samples.

Table 3. Chemical Composition of Initial Crystals Obtained at 36 °C for Both Cooling Rates

	chemical composition of crystals[a]							
	fast cooling rate				slow cooling rate			
acyl C no.	HMF	10% SFO	20% SFO	40% SFO	HMF	10% SFO	20% SFO	40% SFO
C26	0.6	0.4	0.5	0.3	0.8	0.6	0.6	0.6
C28	0.5	0.5	0.4	0.3	0.5	0.4	0.4	0.3
C30	1.0	0.9	0.9	0.6	0.9	0.8	0.8	0.5
C32	2.0	1.8	1.7	1.2	1.9	1.8	1.6	1.1
C34	4.5	4.2	3.9	2.9	4.3	4.1	3.6	2.4
C36	8.8	8.2	7.7	5.8	7.8	7.4	6.6	4.4
C38	10.2	9.6	9.2	7.1	11.7	11.3	10.3	7.3
C40	10.4	9.8	8.9	6.9	7.2	6.8	6.1	4.0
C42	6.2	5.9	5.5	4.2	6.2	5.8	5.2	3.8
C44	7.6	7.1	6.6	5.4	7.5	6.7	6.1	5.1
C46	9.6	9.0	8.2	7.0	9.7	8.4	7.8	7.3
C48	11.3	10.4	9.3	8.2	12.3	10.5	9.9	9.4
C50	13.5	12.5	11.4	10.4	15.3	13.4	12.7	12.5
C52	10.5	10.8	11.6	13.6	9.9	10.1	10.5	12.2
C54	3.2	8.8	14.1	26.0	4.2	11.9	17.8	29.0
C54 (18:0)-d	0.6	0.6	0.4	0.3	0.5	0.6	0.4	0.9
C54 (18:1)-a,b,c	2.6	8.2	13.7	25.7	3.6	11.3	17.5	28.2
C54-b (unknown)	1.2	1.5	1.8	2.9	1.5	2.0	2.3	2.4
C54-c (unknown)	0.8	0.8	0.7	1.0	1.3	1.0	0.9	1.0
C54 (18:1cis)-a	0.6	5.9	11.2	21.8	0.8	8.3	14.3	24.9

[a] Standard deviations for all values were $<\pm 1\%$.

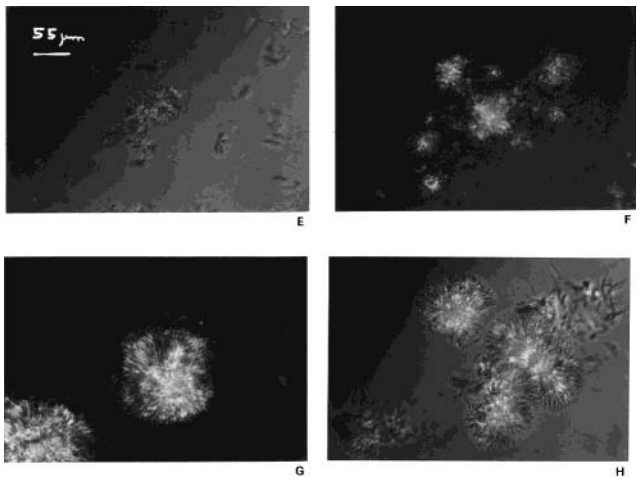

Figure 6. Morphology of initial crystals of samples crystallized to 36.0 °C: (E) 0%, (F) 10%, (G) 20%, and (H) 40% SFO at slow rates (0.1 °C/min).

Figure 6 shows the initial crystals obtained when the samples were crystallized under the same conditions used for Figure 5 but at a cooling rate of 0.1 °C/min. All samples showed spherulitic patterns that were larger and less densely packed with the addition of SFO. The samples with 0 and 10% SFO showed similar morphologies, with only small differences in size for both rates. The samples with 20 and 40% SFO showed greater differences, with larger spherulites indicative of a promotion of crystallization at the slower cooling rate. For high supercoolings, ($\Delta T_{HMF} = 4.2$, $\Delta T_{10\%SFO} = 4.4$), there was only a minor influence of the cooling rate; however, for intermediate ($\Delta T_{20\%SFO} = 2.8$) and low supercoolings ($\Delta T_{40\%SFO} = 1.4$), the slow cooling rate promoted crystallization (for the same crystallization time, more well-formed spherulites were found) and influenced the morphology. In this case, the crystallization process was determined by the thermodynamic driving force (the supercooling), although crystallization was also influenced by kinetic factors such as cooling rate.

Composition of Crystals. To study thermal behavior and chemical composition, crystals obtained at 36.0 °C were filtered after being photographed. Table 3 shows the chemical composition of the first crystals formed for fast and slow cooling rates. The solid fraction remaining on the filter contains TAG from both the crystals and any liquid entrainment. However, no differences in entrainment were found between fast and slow cooling rates in a previous study on milk fat fractionation (*14*). Slowly cooled samples had a slightly lower content of acyl carbon number 40 and a slightly higher content of carbon numbers 50 and 54. The cis-unsaturated component of the C_{54} peak was higher in the slowly cooled sample with 40% SFO than in the rapidly cooled sample. These differences were too small to explain completely the shorter induction times found at the slow cooling rate. Interactions between TAG should also play a key role. Under the conditions of this study, the slowly cooled samples crystallized more rapidly and were less likely to form compound crystals than the rapidly cooled samples. At the fast rate, a TAG with a higher melting point could develop compound crystals (a solid solution) with another TAG, which could have a lower melting point. Breitschuh and Windhab (*15*) reported that compound crystals were formed in milk fat rapidly crystallized when supercooling was performed, even if the supercooling took place only for a short period of time.

Thermal Behavior of Crystals. Figure 7 shows representative DSC thermograms of the crystalline solids obtained for both cooling rates of samples with different SFO contents. For the pure HMF sample at both cooling rates, two endotherms were found with peak temperatures close to 20 and 44 °C. The 20 °C peak decreased in size with increased addition of SFO (10 and 20%) and did not appear in the sample with 40% SFO. This is in agreement with the decrease of short- and medium-chain TAG content with the addition of SFO (Table 1). Thermal behavior changed with cooling rate in all cases. The high-temperature endotherm was broader for the crystals obtained at a slow cooling rate. The peak temperatures of the second endotherms were 43.7 ± 0.6, 42.6 ± 0.5, 42.9 ± 0.8, and 47.1 ± 0.8 °C for the HMF and 10, 20, and 40% SFO samples crystallized at the fast cooling rate, respectively, and 44.1 ± 0.7, 43.0

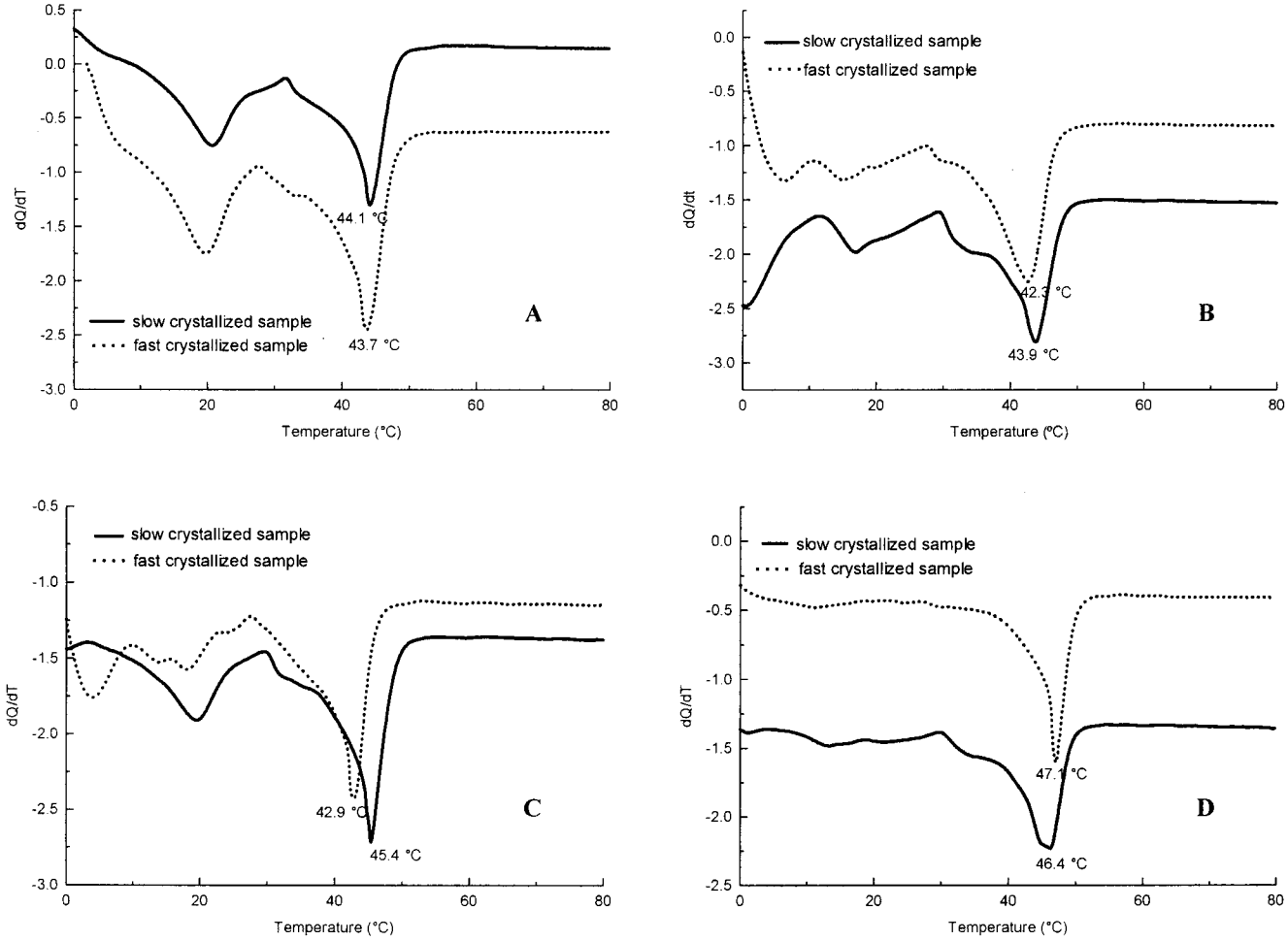

Figure 7. DSC melting diagrams of crystals obtained by dry filtering at 36.0 °C for all samples at slow (0.1 °C/min; solid line) and fast (5.5 °C/min; dotted line) cooling rates. Plots A−D represent 0, 10, 20, and 40% addition of SFO to HMF.

± 0.8, 45.4 ± 0.8, and 46.4 ± 0.7 °C for these samples crystallized at the slow cooling rate. Enthalpies of the high-temperature endotherm were 52.2 ± 9.2, 52.2 ± 8.6, 53.9 ± 9.1, and 63.1 ± 9.5 J/g for the HMF and 10, 20, and 40% SFO samples crystallized at 5.5 °C/min, respectively, and 43.9 ± 8.2, 45.6 ± 8.4, 53.9 ± 8.9, and 52.2 ± 9.0 J/g for those samples cooled at 0.1 °C/min. Neither peak temperature nor enthalpy was different between cooling rates ($p < 0.05$). In addition, no endotherms with higher peak temperature appeared at the slow cooling rate, as would have happened if the polymorphic transition had occurred. For both fast and slow cooling rates, the β'-form was very stable, and crystals remained in this polymorphic form for at least 1 week after storage at 10 °C.

At slow crystallization kinetics, the melting temperature range of the crystals was broader. A wider high-temperature peak was observed for all slowly crystallized samples (Figure 7). The way in which the profile was modified suggests that the differences found in melting curves were most likely not due to a polymorphic transition but due to differences in chemical composition and phase behavior of the mixed TAG.

Two important phenomena that influence the crystallization of natural fats are polymorphism and intersolubility (the interactions between TAG when they crystallize). In the present study, it was demonstrated that polymorphism does not explain the differences in crystallization behavior of milk fat−vegetable oil blends because the polymorphic form obtained was the same for all blends at all T_c. The cooling rate influenced the intersolubility of TAGs so that different solid solutions, eutectics, or compound crystals were formed, which showed different thermal behaviors. This may be related to the time and temperature at which molecular organization took place prior to nuclei formation. In rapidly cooled systems, molecular organization took place at a lower temperature than in slowly cooled systems, in which molecular organization took place as the sample was cooling to T_c. Thus, the time scales for nucleation were different between the different cooling rates, and the crystal compositions (and melting profile) of the final product also were different.

ABBREVIATIONS USED

HMF, high-melting milk fat fraction; SFO, sunflower oil; T_m, melting point; MDP, Mettler dropping point; TAG, triacylglycerols; T_c, crystallization temperature; τ, induction time.

ACKNOWLEDGMENT

We are grateful to Yuping Shi for chromatographic analysis.

LITERATURE CITED

(1) Swaisgood, H. E. Characteristics of edible fluids of animal origin: milk. In *Food Chemistry*; Fennema, O. R., Ed.; Dekker: New York, 1985; pp 791−828.

(2) Kaylegian, K. E.; Lindsay, R. C. Application of milk fat fractions in food. In *Handbook of Milkfat Fractionation Technology and Application*; AOCS Press: Champaign, IL, 1995; pp 525−630.
(3) Garside, J. General principles of crystallization. In *Food Structure and Behavior*; Blanshard, J. M. V., Lillford, P., Eds.; Academic Press: London, U.K., 1987; pp 35−49.
(4) Boistelle, R. Fundamentals of nucleation and crystal growth. In *Crystallization and Polymorphism of Fats and Fatty Acids*; Garti, N., Sato, K., Eds.; Dekker: New York, 1988; pp 189−226.
(5) Ng, W. L. A study of the kinetics of nucleation in a palm oil melt. *J. Am. Oil Chem. Soc.* **1990**, *67*, 879−882.
(6) Herrera, M. L.; Falabella, C.; Melgarejo, M., Añón, M. C. Isothermal crystallization of hydrogenated sunflower oil: I—Nucleation. *J. Am. Oil Chem. Soc.* **1998**, *75*, 1273−1280.
(7) Herrera, M. L.; de León Gatti, M.; Hartel, R. W. A kinetic analysis of crystallization of a milk fat model system. *Food Res. Int.* **1999**, *32*, 289−298.
(8) Toro-Vazquez, J. F.; Briceño-Montelongo, M.; Dibildox-Alvarado, E.; Charó-Alonso, M.; Reyes-Hernandez, J. Crystallization kinetics of palm stearin in blends with sesame seed oil. *J. Am. Oil Chem. Soc.* **2000**, *77*, 297−310.
(9) Herrera, M. L. Crystallization behavior of hydrogenated sunflowerseed oil: kinetics and polymorphism. *J. Am. Chem. Soc.* **1994**, *71*, 1255−1260.
(10) Lund, P. Butterfat triglycerides. *Milchwissenschaft* **1988**, *43*, 159−161.
(11) Strickland-Constable, R. F. Nucleation of solids. In *Kinetics and Mechanism of Crystallization*; Academic Press: London, U.K., 1968; pp 74−129.
(12) Sato, K. Crystallization of fats and fatty acids. In *Crystallization and Polymorphism of Fats and Fatty Acids*; Garti, N., Sato, K., Eds.; Dekker: New York, 1988; pp 254−259.
(13) Chong, C. L.; Sato, K. Kinetic study of palm oil crystallization. *Int. News Fats, Oils Relat. Mater.* **1993**, *4*, 537.
(14) Patience, D. B.; Hartel, R. W.; Illingworth, D. Crystallization and pressure filtration of anhydrous milk fat: mixing effects. *J. Am. Oil Chem. Soc.* **1999**, *76*, 585−594.
(15) Breitschuh, B.; Windhab, E. J. Parameter influencing co-crystallization and polymorphism in milk fat. *J. Am. Oil Chem. Soc.* **1998**, *75*, 897−904.

Received for review September 6, 2000. Revised manuscript received May 1, 2001. Accepted May 7, 2001. S.M. is grateful to the National Research Council of Argentina for a Ph.D. scholarship. This work was supported by the National University of La Plata through Project 11/X279.

JF001101J